Moving Boundaries: An Eulerian Approach

James M. Brethour
Flow Science, Inc.
Santa Fe, New Mexico, USA 87505

Abstract

For many problems, it is advantageous to maintain a grid which is fixed in space while allowing internal boundaries of the fluid and/or solid regions to move within it. This is appropriate wherever drastic changes in the conformation of these boundaries occur, as the necessity of remeshing is avoided. Mesh generation is also greatly simplified. Various approaches are shown to model the boundary movement of the fluid interface, sediment, solidified fluid, and elastic materials within the fixed grid. The movement of fluid boundaries is accomplished with a variant of the Volume-of-Fluid (VOF) method whereby a quantity representing the amount of fluid in each of the computational cells is advected through the fixed mesh. Erosion and deposition of sediment is computed by means of a sediment scour model; the local rate of erosion is based on the local shear stress present at the packed sediment/fluid interface, and deposition is predicted with a Stokes flow approximation. The packed bed interface conforms according to the sediment concentration and the packing fraction of the sediment. Molten metal can solidify as the temperature drops below its freezing point. The solidified "fluid" is then treated just like a solid whose surface grows or shrinks as determined from the amount of heat flux causing freezing and/or melting. Elastic stresses are computed in solidified regions by the addition of an elastic stress computation into the momentum balance within the same fixed grid with the VOF method predicting the solidified material/air interface.

1 Introduction

For highly transient flow problems, the fluid interface, whether it be between fluid and void space or between two immiscible fluids, must move freely according to the dynamics of the problem. One solution would be to create a mesh that deforms along with the interface. This works well for situations where the conformation of the interface changes little during the simulation. However, for more general cases, either a new mesh must be repeatedly created during the simulation, or a method to produce the free surface boundary within an unchanging mesh is needed. This work presents the latter; a Volume-of-fluid (VOF) function is used to track the location of the free surface. Additionally, this function is used to compute curvature to predict the effects of surface tension. Of interest to coating engineers, this work presents the filling and

emptying of an individual gravure cell as an example; a gravure cell is a tiny pit etched into the surface of a metal roller the purpose of which is to transfer a measured amount of coating fluid onto a substrate or transfer roll.

Another moving boundary problem that commonly occurs in hydraulics problems is the erosion and deposition of sediments. The packed sediment acts as a solid whose surface is dependent on the local conditions of the overlying fluid. In regions where the local shear stress is large, erosive action causes a gradual removal of the sediment, while elsewhere, this sediment may be redeposited, causing a thickening of the packed bed. This work presents the erosion of sand in a flume as validation and scour around a bridge pier as an example.

Deformable solids or plastically deforming materials are modeled with an elastic-plastic model; an additional term added to the momentum equation includes the elastic stress. This is computed on the same fixed grid, with the local components of the stress tensor advected with the material as it moves and/or deforms. Again, the volume-of-fluid function tracks the interface of these solid-like regions. Additionally, localized yielding of the elastic material can occur; the Mises Yield Condition [1] is used to predict such plastic flows.

All of the simulations presented here were computed using the control-volume-VOF method as it has been implemented in the commercial software package ***FLOW-3D***® developed by Flow Science, Inc., Santa Fe, New Mexico, USA [2].

2 Moving fluid and solid boundaries – filling and emptying of a gravure cell

Within the grid of finite control volume elements, one gravure cell was created by blocking off flow to elements located within solid regions, and elements are partially blocked to flow by manipulating the area fractions open to flow in each of the three Cartesian directions. A quadrangular gravure cell was used for the simulations. The cell corresponds to a gravure roll where the spacing between each cell is $130\mu m$ and the depth of each cell is $32\mu m$. The cell volume per unit area (V_c) is $13.25\times10^6 m^3/m^2$ and the open fraction of roll surface area is 0.809 (i.e. the fractional area that is composed of the cell openings). Also created

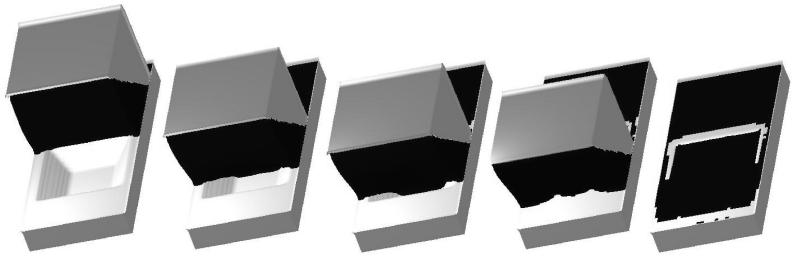

Figure 1. Three-dimensional view of a quadrangular gravure cell filling at $1 m/s$. The elapsed time here is $400\mu s$.

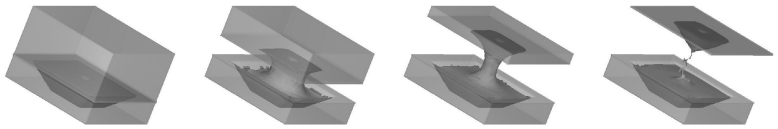

Figure 2. Emptying of gravure cell (same cell dimensions as filling case); a three-dimensional perspective is shown. The transfer roll surface (block at top) is moving away from the gravure roll at 0.5*m/s*. The static contact of the fluid with all surfaces is 30°. The elapsed time is 150μs.

within the mesh is a rigid solid blade, which is translated parallel to the roll surface in the filling simulation. The fluid's viscosity is 10*mPa·s*, its density is 1g/cm^3 and the air-liquid surface tension is 40*mN/m*. The static contact angle between the liquid and the blade is 30° for all cases, while the static contact angle between the liquid and the gravure roll surface is varied.

Figure 1 shows the time evolution of the cell filling process; the static contact angle with the gravure roll is 30°, the roller speed is 1*m/s* and the gap between the blade and the gravure roll is 2μm. In this case, the advancing contact line at the front edge of the liquid bead is able to move into the gravure cell quickly enough so that air is not trapped by the leading edge of liquid entering the cell. After the blade had passed over the cell, the liquid overlying the cell edges thins due to the capillary pressure driving fluid away under the curved surface. Greatest fill fractions are obtained at low roll speeds and low static contact angles (with the gravure roll surface). Low roll speeds allow the advancing contact line to enter farther into the cell before can be air trapped by the action of the blade. Low contact angles result in faster advancement of the contact line.

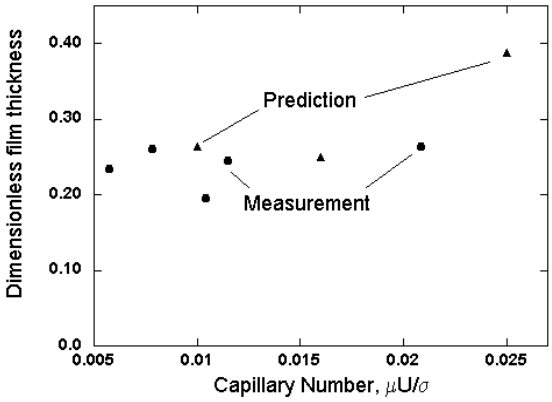

Figure 3: Comparison between computational simulation and experimental measurement [3] of cell emptying effectiveness as a function of capillary number.

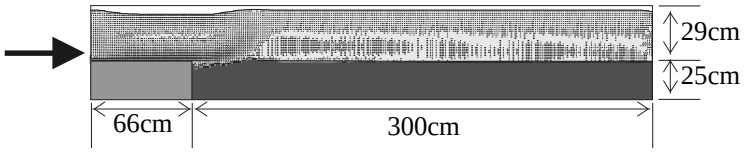

Figure 4: Profile of experimental flume setup for submerged horizontal jet problem [4].

The emptying process is simulated by the pulling away of the substrate from the gravure roll surface; this was accomplished by creating a solid blade that translates linearly away from the roll. This motion is adequate to describe the separation at such small scales. Also the initial condition of the liquid within the gravure cell was presumed from the results of the gravure filling simulations. Figure 2 shows the case where the transfer roll is pulling away at 0.5m/s and the static contact angle with all surfaces is 30°. These results show the necking and breakoff of the liquid as it pulls away from the gravure cells. A fraction of the liquid adheres to the transfer roll. Also, higher speeds and/or higher contact angles cause the volume of fluid adhering to the transfer roll to fall. Results favorably comparing this applied fraction to experimental measurement of film thickness are shown in Figure 3.

3 Prediction of a packed sediment interface

The approach taken is this work is to incorporate a fully three-dimensional fluid model coupled with a continuously changing packed bed interface. Sediment is treated as a continuum; a concentration is stored which relates to the number of sediment particles in a volume of fluid. The two components of scour, drifting and lifting, are superimposed on the advection of sediment by the fluid. Regions where the sediment concentration reaches the packing limit exhibit solid-like behavior. The effects of slope of the packed bed interface are included.

The sediment particles are presumed to be small relative to the scale of the flow. In regions where the sediment is suspended in the fluid, the sediment advects with the fluid flow. The advection of sediment is computed from

$$\frac{\partial C_s}{\partial t} + \nabla \cdot (\mathbf{u} C_s) = Diffusion\,terms \qquad (1)$$

where C_s is the local concentration of sediment. The fluid density is computed as the volume-weighted average of the fluid and sediment, and this density is used in the conservation of momentum equations for the fluid flow. The Renormalization-Group method for formation and dissipation of turbulent energy is incorporated into the flow model [6,7]. The presence of sediment does not affect the formation or dissipation of turbulent energy, but the turbulent energy can affect the diffusion of sediment; this is included in the right side of Equation 1.

Additionally, sediment particles drift relative to the fluid due to the density difference between the sediment particles and the fluid. The drift velocity is computed as the balance between buoyancy and the fluid's drag on the particle.

The drag is computed with the assumption of Stokes flow around spherical particles and buoyancy is computed from the mechanical potential gradient so as to include effects of centripetal acceleration in flow with curving streamlines. The resulting drift velocity is

$$\mathbf{u}_{drift} = \frac{d^2\left(\rho_s - \rho_f\right)}{18\mu} \underbrace{\frac{\nabla P}{\overline{\rho}}}_{\substack{\text{Mechanical potential} \\ \text{gradient}}} . \tag{2}$$

Here u_{drift} is the velocity of the fluid particle relative to the fluid, d is the average particle diameter, μ is the local fluid viscosity (which includes effects due to turbulence), ρ_f and ρ_s are the fluid and microscopic particle densities, respectively, ∇P is the local pressure gradient and $\overline{\rho}$ is the local mean density.

In regions where the sediment drifts and accumulates (e.g. on the inside curve of a meandering stream), the suspended sediment becomes *packed sediment*, which does not advect with the fluid; fluid flow ceases in these regions. However, packed sediment can be re-suspended into the fluid if the shear stress at the packed bed – fluid interface is sufficient to pick up the sediment particles. In turbulent flow, the shear stress is enhanced by the local turbulent kinetic energy. The lift velocity is computed as

$$u_{lift} = \alpha\sqrt{\frac{\tau - \tau_{crit}}{\overline{\rho}}} \tag{3}$$

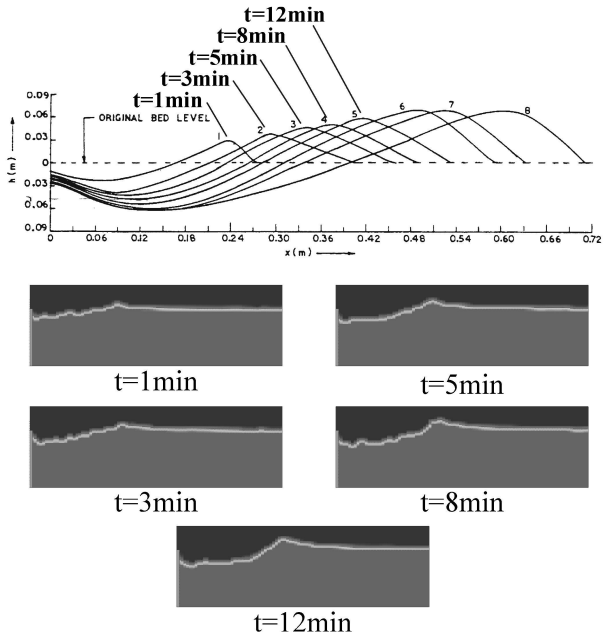

Figure 5: Top plot shows the time evolution of the packed bed profile based on experiment [4]. The bottom plots show the predicted profiles of the packed sediment bed.

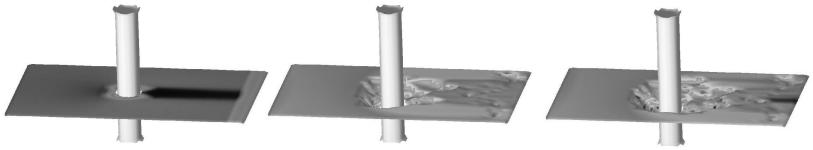

t=0min t=6min t=12min

Figure 6: Time evolution of the formation of a scour hole around the base of a cylindrical pier. The surface shown is the packed bed interface; the water is flowing from left to right over this surface. Such catastrophic erosion could occur during a flood. The shading represents the magnitude of the strain rate at the packed bed interface.

where α is a probability parameter, τ is the local shear stress at the packed bed interface, and τ_{crit} is the critical shear stress. In areas on the packed bed interface where τ is less than τ_{crit}, no scour lift occurs. The direction of u_{lift} is always away from the packed bed interface. The rationale behind this empirical model is that $\sqrt{\tau/\rho}$ is the *shear velocity* [7], which is a measure of the velocity within the boundary layer. The scour parameter α is the probability that a sediment particle on the packed bed interface is lifted away; its value is typically close to 1. Also, α can be increased to model qualitative behaviour on an accelerated time frame. τ_{crit} is calculated from the critical Shields Parameter, θ_{crit}:

$$\tau_{crit} = \theta_{crit} g(\rho_s - \rho_f) d \,. \tag{4}$$

Here g is the magnitude of the gravity vector, **g**. θ_{crit} is found in the literature for various materials; typical values range from 0.03 to 0.05.

The model was tested with experimental flume data; a submerged horizontal planar jet issues from a 2*cm* wide slit under a pressure of 11.8*cm* H_2O to produce a steady-state velocity of 175*cm/s*. The planar jet flows over the surface of a solid apron, 66*cm* long. Beyond the apron, the bed of sand extends for 3*m* lengthwise, 25*cm* deep and 60*cm* wide. All measurements were made in the centerline of the flume, so the profile is taken to be two-dimensional. The average particle diameter of the sand is 0.76*mm* and its specific gravity is 2.65. The Shields parameter was taken to be 0.04 in this system [4]. A finite difference approximation of the sediment transport equation was used to predict advection of the suspended sediment. Figure 4 shows a two-dimensional slice of the flume setup. Figure 5 shows the packed sediment bed profiles after 1, 3, 5, 8 and 12 minutes of scour, along with the experimentally measured profiles [4]. The predicted packed sand bed profile compares well in the time evolution to that of the experiments. The trough and ridge both move downstream with time while the trough deepens and the ridge grows. Also, the ridge peak becomes less sharp as time advances, just as observed during the flume studies.

Figure 6 shows the results of the three-dimensional simulation of scour around a bridge abutment. In this case, the sand used has the same properties of the aforementioned flume study, and the pier has a diameter of 2*m*. The sediment for this simulation has the same properties as the aforementioned flume

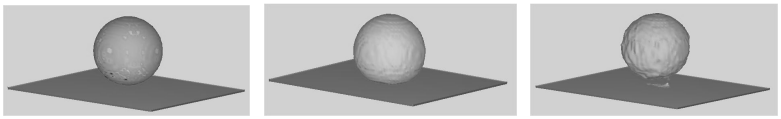

t=0.0 s t=0.02 s t=0.07 s

Figure 7: Simulation of a sphere striking a solid surface. Sphere is simulated as an elastic material whose shear modulus is 10*kPa* and the density is 1g/cm^3. Yielding is not permitted in this example.

experiments. The scour holes produced by the simulation have a shape that has been observed experimentally [8].

4 Deformation of elastic materials

The model incorporates elastic stress as an additional stress within the material. That is, the total state of stress is a summation of pressure, viscous and elastic stresses. At a particular point in time, t, for an element of material, the elastic stress is

$$\boldsymbol{\tau}_E(\xi,t) = \int_{-\infty}^{t} 2G\dot{\mathbf{E}}(\xi,t')dt' \tag{5}$$

where τ_E is the elastic stress tensor, G is the elastic modulus, and $\dot{\mathbf{E}}$ is the local strain rate tensor. Since τ_E is a material property, ξ represents a particular element of the material. Equation 5 is the basis of the stress model. The current value of stress is a function of the past history of the material element. Material entering from the boundaries is assumed to have a zero state of elastic stress. Also, fluid initially in the domain at time zero has a zero state of elastic stress. For finite time steps, Equation 5 can be rewritten and is

$$\boldsymbol{\tau}_E(t) = \sum_{i=1}^{n} 2G\dot{\mathbf{E}}_i \Delta t_i \tag{6}$$

which forms the basis of the incremental stress model. Here $\dot{\mathbf{E}}_i$ is the strain rate tensor at time step i, and Δt_i is the time step at time step i. The components of τ_E

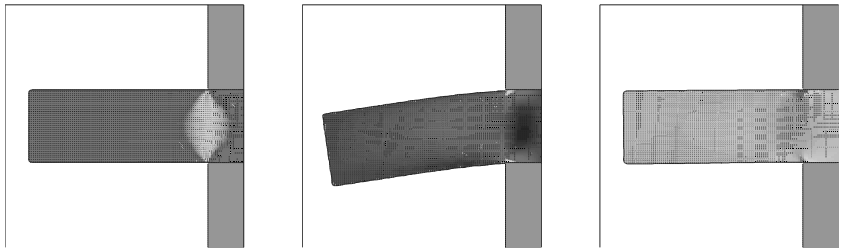

t=0.0005 s t=0.0195 s t=0.0395 s

Figure 8: Simulation of flexing beam due to gravity. This is an example of the large deformation capabilities of the model. The beam is an elastic material with shear modulus 10*kPa*, density 1g/cm^3, thickness 0.3*cm*, and length (from the wall surface) 0.75*cm*.

advect with the material; this is described by

$$\left(\frac{\partial \boldsymbol{\tau}_{\mathbf{E}}}{\partial t}\right)_x + \mathbf{u}\cdot\nabla\boldsymbol{\tau}_{\mathbf{E}} = 0 \ . \tag{7}$$

Figure 7 shows an example problem where elastic stress dominates – i.e. the material behaves like an elastic solid. This simulation shows a solid sphere which bounces elastically off a solid surface. Figure 8 shows another example where an elastic beam is flexing due to the effect of gravity. The beam oscillates before reaching equilibrium; the frequency of this oscillation matches well to the analytical frequency of the primary mode of vibration. Figure 9 shows a case

t=0.005 s t=0.015 s t=0.035 s

Figure 9: Simulation of extrusion of plastically yielding material from a cylindrical extruder. The material viscosity is 0.05*Pa·s*, its shear modulus is 10*kPa*, and the yield stress is 10*kPa*. The extruder opening is 4 cm in diameter.

where a plastically deforming (Bingham) material is issuing from an extruder.

5 Summary

This work has shown several instances where fixed-grid methods are a viable alternative for solving moving and deforming boundary problems. The Volume-of-fluid method is a tried and true approach to simulate free surfaces; improvements still continue to be made in the accuracy of the fluid advection to minimize fluid loss, and the calculation of curvature for flows that require the effects of surface tension. A more novel approach for fixed-grid methods is the prediction of the erosion of packed sediment and elastic solids. For packed sediment, a concentration is used to predict which regions are packed (i.e. solid-like) or not. As a velocity need not be computed within the packed region, an accurate measure of the overlying fluid velocity can still be maintained. Elastic solids posed additional challenges to the control volume-VOF method; the components of elastic stress must be advected with the movement of the material and also the stress is computed incrementally to allow for non-linear deformations with a simple linear constitutive model. What has been shown is that all of these diverse problems can be solved by simple numberical approaches

within fixed grids. These boundaries can behave in very complex ways without the associated mesh generation challenges.

References

[1] Malvern, L.E. *Introduction to the Mechanics of a Continuous Medium*, Prentice-Hall: Upper Saddle River, NJ, 1969.

[2] ***FLOW-3D***® User's Manual, Flow Science, Inc. report FSI-02-1 (2002), www.flow3d.com.

[3] Benkreira, H. & Patel, R. Direct gravure roll coating. *Chemical Engineering Science*, **48(12)**, pp. 2329-2335, 1993.

[4] Chatterjee, S.S., Ghosh, S.N. & Chatterjee, M. Local scour due to submerged horizontal jet. Journal of Hydraulic Engineering 120(8), pp. 973-992, 1994.

[5] Yakhot, V. & Nakayama, P.I. Renormalization group analysis of turbulence. I. Basic theory. *Journal of Scientific Computing* **1**, pp. 1-51, 1986.

[6] Yakhot, V. & Smith, L.M. The renormalization group, the ε-expansion and derivation of turbulence models. *Journal of Scientific Computing* 7, pp. 35-61, 1992.

[7] Lyn, D.A. Sediment transport in open channels (Chapter 33). *The civil engineering handbook*, ed. W.F. Chen, CRC Press: Boca Raton, FL, pp. 1070-1088, 1995.

[8] Melville, B.W. & Raudkivi, A.J. Flow characteristics in local scour at bridge piers. Journal of Hydralic Research 15(4), pp. 373-380, 1977.